Numerical Analysis of Prestressed Concrete Bridge Girders Failing in Shear

Mustafa, S.; Lantsoght, E.O.L.; Yang, Y.; Sliedrecht, Henk

DOI
10.14359/51736109

Publication date
2022

Document Version
Final published version

Published in
ACI Structural Journal

ACI STRUCTURAL JOURNAL TECHNICAL PAPER

Title No. 119-S128

Numerical Analysis of Prestressed Concrete Bridge Girders Failing in Shear

by Shozab Mustafa, Eva O. L. Lantsoght, Yuguang Yang, and Henk Sliedrecht

The safety of existing slab-between-girder bridges is subject to discussion in the Netherlands. Current design codes are conservative for shear-critical girders, and nonlinear finite element analysis is considered a more accurate assessment method. This paper investigates if the Dutch guidelines for nonlinear finite element analysis, which were largely based on laboratory experiments, can safely predict the behavior of large-scale shear-critical post-tensioned girders. The simulation results are compared with experimental observations on girders taken from a demolished bridge (the Helperzoom bridge) after serving for more than 50 years. Predicted and experimentally observed material properties are used as inputs for numerical models. For both, safe predictions of inclined cracking and ultimate capacities are obtained. Parameter studies for load positions and prestress levels are also performed to get a deeper insight into the structural behavior of such girders. This work shows that the guidelines can be used for assessment.

Keywords: bridge assessment; concrete bridges; finite element analysis; flexural shear; prestressed concrete; shear; shear-compression; shear-tension.

INTRODUCTION

In the Netherlands, many existing prestressed concrete bridges built during the 1960s and 1970s require assessment. The intensity and frequency of traffic loads have increased since the design and construction of these bridges, and the recently introduced Eurocode 2, NEN-EN 1992-1-1+C2 (European Committee for Standardization 2011), requirements result in lower shear capacities than previously used national codes. Therefore, there are concerns regarding the safety of these existing bridges.

The reconstruction of the perimeter around the city of Groningen in the Netherlands presented an opportunity to test actual bridge girders (sawn at half of the length to facilitate transportation and handling in the laboratory) from a demolished bridge, the Helperzoom bridge, and to gain insights into the shear behavior of these girders (Lantsoght et al. 2021). The Helperzoom bridge was constructed in the 1960s, and the stirrups of the bridge girders consist of plain bars that follow the bulb-T-shape of the girder. This detail is not accepted in modern design codes. Besides, after more than 50 years, the remaining prestress level of the bridge is unclear; thus, the potential beneficial effect of prestressing on the shear resistance of the girder cannot be accurately accounted for. These aspects are typical for existing post-tensioned girders, and they introduce additional challenges in assessing their capacity and critical failure mode.

When the assessment based on code equations indicates that the girder does not fulfill the code requirements, a higher Level of Approximation can be used. The philosophy of levels of increasing computational time and effort to obtain higher accuracy, called Levels of Approximation, was first introduced in the *fib* Model Code 2010 (*fib* 2012). The expectation is that increasing Levels of Approximation will approach the tested capacity of a structural member, taking an appropriate safety margin into account. From this perspective, nonlinear finite element analysis can be used as a higher Level-of-Approximation approach for the assessment of the existing prestressed concrete bridges.

In the Netherlands, RTD 1016-1:2020, Guidelines for Nonlinear Finite Element Analysis of Concrete Structures (Rijkswaterstaat 2020a), was published by the Dutch Ministry of Infrastructure and Water Management to support the numerical modeling of existing and new concrete structures with complex loading conditions or failure modes. The guidelines have been systematically validated for typical structural types, namely reinforced concrete beams in RTD 1016-3A:2017 (Rijkswaterstaat 2017a), prestressed beams in RTD 1016-3B:2017 (Rijkswaterstaat 2017b), reinforced concrete slabs in RTD 1016-3C:2017 (Rijkswaterstaat 2017c), and prestressed beams following the updated guidelines in RTD 1016-3D:2020 (Rijkswaterstaat 2020b). As these validation studies mostly focus on validating experiments on laboratory-made members with well-defined material properties and construction details, it is often questioned if the RTD 1016 suite still applies for the assessment of existing structures.

The experimental research on the Helperzoom girders offers a unique opportunity to validate the Dutch guidelines using test data of a real existing structural member, including all the complex details and aging of the material. The experimental results are used as a benchmark to assess the accuracy of numerical models following the RTD 1016 provisions. Numerical models are also developed following the results of a material investigation on the Helperzoom girders for comparison with the RTD models. The verified models are then used to further explore the influence of parameters that were studied in the laboratory for a limited range of input values, and thus extend the understanding of the behavior of these girders.

ACI Structural Journal, V. 119, No. 6, November 2022.

MS No. S-2021-216.R1, doi: 10.14359/51736109, received March 8, 2022, and reviewed under Institute publication policies.

RESEARCH SIGNIFICANCE

This paper shows the comparison between complex experiments and nonlinear finite element models. The research significance consists of: 1) showing that the Dutch guidelines for nonlinear finite element analysis lead to accurate and safe results for complex experiments, and thus can be used for the assessment of existing prestressed bridges (post-tensioned girders in slab-between-girder bridges, slab-on-girder bridges, as well as box-girder bridges); and 2) carrying out additional parameter studies to extend the experimental results and gain additional insight into the behavior of prestressed girders.

DUTCH GUIDELINES FOR NONLINEAR FINITE ELEMENT ANALYSIS

In the Netherlands, the Guidelines for Nonlinear Finite Element Analysis of Concrete Structures (RTD 1016-1:2020) (Rijkswaterstaat 2020a) outlines the modeling aspects, and RTD 1006:2013 (referred to as "RBK" from the Dutch name, "Guidelines for the Assessment of Bridges") (Rijkswaterstaat 2013) outlines the assumptions for the assessment of existing concrete bridges owned by the Dutch Ministry of Infrastructure and Water Management. The RTD 1016-1:2020 guidelines provide a set of recommendations to assist the users of nonlinear finite element models in choosing the material properties, modeling parameters, and so on for concrete structures. The target of the guideline is to provide a similar prediction among various users and applications, which is sufficiently accurate without requiring unrealistic computational effort. To ensure the target reliability level for assessment at the ultimate limit state, the guideline adapted a so-called Global Resistance Factor (GRF) method (de Boer et al. 2014; Pimentel et al. 2014; Schlune 2011). The GRF approach considers the uncertainties of the material properties and the model together with a GRF. The uncertainty levels of different materials, like concrete and steel, are considered by adjusting the model input of the material properties.

The background report RTD 1016-3B:2017 (Rijkswaterstaat 2017b) to the RTD 1016-1:2017 guidelines shows the verification of the proposed approach for modeling prestressed girders. In this background report, four classic experiments from the literature were modeled following the recommendations from RTD 1016-1:2017. The four experiments are taken from three different references, with two experiments from Germany (Leonhard et al. 1973) and two experiments from the United States (Sun and Kuchma 2007; Runzell et al. 2007). The failure mechanisms that were successfully predicted were flexural failure with crushing of the concrete compression zone, shear-compression failure for a beam under a distributed load, and two cases of shear-compression failure for a beam under a concentrated load. These studies also showed the validity of the approach using different safety formats, such as the GRF (Belletti et al. 2013b; Blomfors et al. 2016; Schlune 2011; Schlune et al. 2011). Extensive work has been done in developing the RTD guidelines using different commercial finite elements packages (Belletti et al. 2013a; Rijkswaterstaat 2017a) so that the user can be helped in deciding the numerical parameters like mesh size, type of finite element, material behavior, and so on. Moreover, the approach from RTD 1016-1:2017 has also been successfully applied on full-scale field tests to collapse a prestressed concrete slab-between-girder bridge (Ensink et al. 2019).

Despite successful simulations of full-scale tests reported in the literature (Zwicky and Vogel 2000; Zwicky 2002), there are still concerns about the accuracy of nonlinear finite element methods, especially when they are applied to evaluate the shear failure of large members without or with limited shear reinforcement. The recent shear-prediction contest organized by Delft University of Technology (Yang et al. 2021) also showed that numerical models can lead to a wide variety of different predictions by different users. Because many of the existing prestressed girders in the Netherlands were designed based on the principal stresses, the amount of shear reinforcement in the web is typically low. Additionally, the limited shear reinforcement applied in the existing prestressing girders often does not fulfill modern detailing requirements. A typical example of such a non-code-compliant stirrup design is found in the Helperzoom bridge girders, as shown in Fig. 1(a) and (b). It is often questioned if these structures can be assessed with the recommended nonlinear finite element approach.

This study focuses on the application of RTD 1016-1:2020 and RBK, as the ultimate goal of this research is the improvement of assessment procedures for slab-between-girder bridges in the Netherlands. Additionally, the Dutch guideline can serve as a basis for the development of international codes.

SUMMARY OF EXPERIMENTS

A companion paper (Lantsoght et al. 2021) describes the experiments on the Helperzoom girders and details the conclusions from these experiments in terms of shear cracking and shear failure. In this section, a summary of the experiments is provided for the background of the associated finite element models. The girder specimens are identified as HPZ01 to HPZ04, referring to the four specimens obtained from the demolished Helperzoom bridge. The specimens are obtained after sawing the original girders in half to facilitate transportation and handling in the laboratory. Because of the coarse action of sawing, the girders vary in length from 10.51 to 12.88 m (34.48 to 42.25 ft). The span length used in the laboratory for testing is 9.60 m (31.49 ft) in all four experiments. All the girders have a height of 1.11 m (3.64 ft). The girders have draped tendons, with some tendons anchored at the top flange and the majority of the tendons anchored in an anchor block (full cross section at the end of the girder), as shown in Fig. 1(c). The cross-sectional width is tapered in the transition away from the anchor block to the bulb-T cross section. In the bridge, diaphragm beams are used at the support and at one-third of the span length. These beams were cut to isolate the HPZ girders.

Two load positions are used in the experiments: at 2.903 m (9.52 ft) from the center of the support (HPZ01 and HPZ02) and at 4.40 m (14.44 ft) from the center of the support (HPZ03 and HPZ04). The sequence of cracking in the experiments is flexural cracking, inclined (shear)

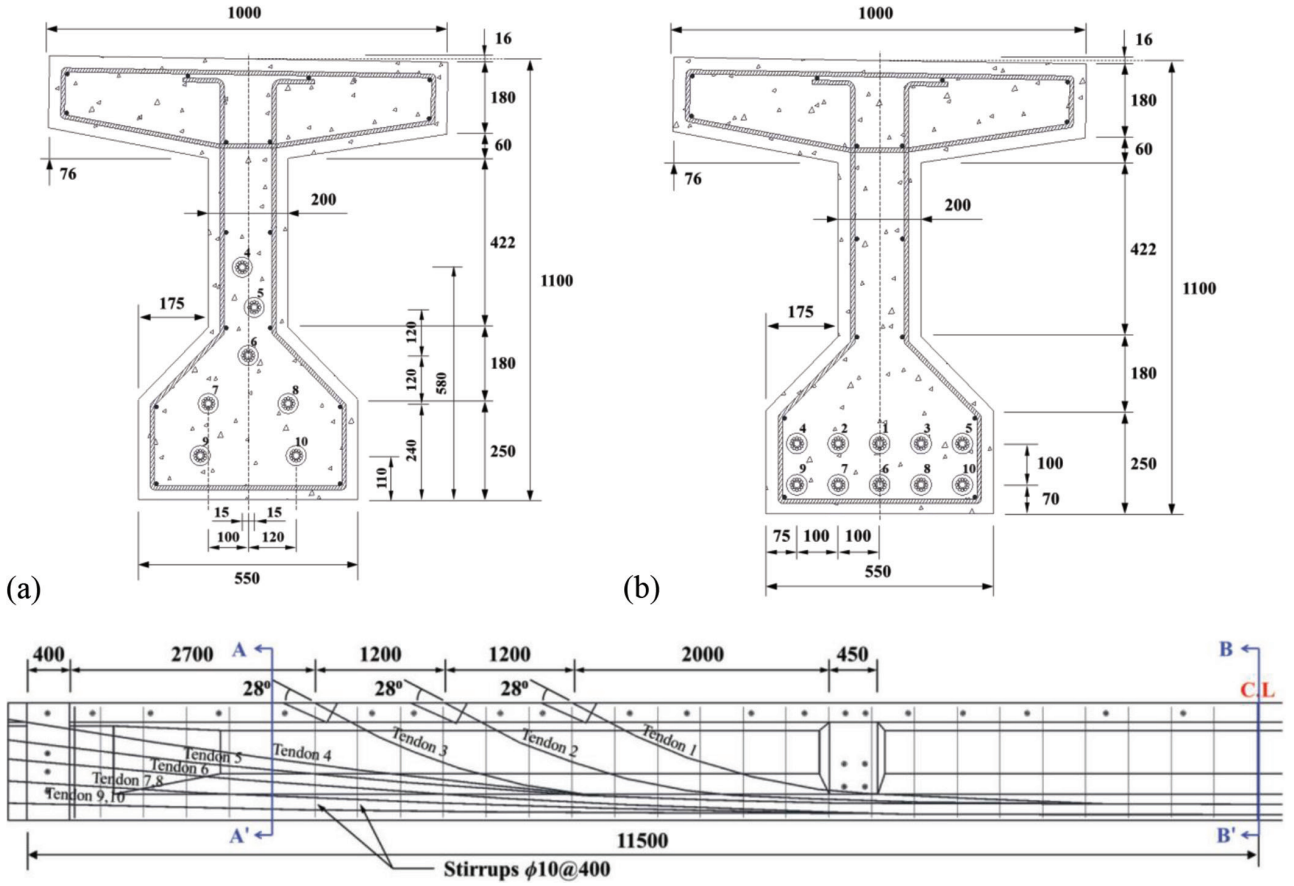

Fig. 1—Cross section of: (a) girder at section A-A'; (b) girder at section B-B'; and (c) longitudinal section of girder with tendon layout and definition of sections A-A' and B-B'. (Note: Dimensions in mm; 1 mm = 0.04 in.)

cracking, and ultimate failure. A significant load increase between the inclined cracking load and the ultimate load happened in all the experiments, showing the activation of the non-code-compliant stirrups. In all the experiments, flexure-shear cracking was observed before shear-tension cracking.

The concrete compressive strength and tensile strength are determined based on concrete cores taken from the girders. The properties of the mild steel and the prestressing steel are obtained in the laboratory by means of a tensile test. The Young's modulus of the concrete is determined by taking additional core samples from the girder specimens after testing. The level of prestressing is measured by: 1) drilling cores and measuring the strain change; 2) cutting the prestressing strands and measuring the change in strains; and 3) evaluating the cracking load in the experiment using the load-displacement diagram, and comparing a layered sectional model and Response-2000 (Bentz 2000) to the experimental results for different values of prestressing. All the details of the material properties, test observations, and loads at flexural cracking, inclined cracking, and failure are outlined in the experimental paper (Lantsoght et al. 2021). Relevant values are repeated in the next sections for comparison with the results of the numerical simulations.

FINITE ELEMENT MODEL

Brief description of RTD guidelines

For two-dimensional (2-D) concrete beam simulations, an eight-node quadrilateral element with quadratic interpolation of the displacement field is recommended. The maximum allowable mesh size is the minimum of $L/50$ and $h/6$, where L is the span of the beam and h is the height. For I-shaped beams, h should be interpreted as the height of the web or flange, depending on the region of interest. The loading and support plates are recommended to be modeled using an interface between the plate and the concrete such that the local stress concentrations can be avoided. The horizontal stiffness of the interface should be relatively low to avoid friction.

For reinforcement, embedded models are preferred because they do not require altering the concrete nodes, which should be done when modeling reinforcing bars as separate truss elements. A bond-slip relation may be used to model the concrete-reinforcing bar interaction, or motivation for not using the slip relation should be provided.

For the constitutive model, a parabolic softening curve in compression and an exponential softening curve in tension are recommended for concrete with a total strain-based cracking approach and a rotating crack model. Both the reinforcing and prestressing steel can be modeled with a bilinear approximation of the isotropic hardening behavior.

Overview of numerical models

Eight numerical models are developed in total. Four of these models use the results of material investigations on the Helperzoom girders as input, indicated as "Experimental" material model in Table 1. In addition, for both the shear spans of 2.903 and 4.40 m (9.52 and 14.43 ft), two additional models are developed following the provisions of RTD 1006:2013 (RBK). These models are predictive models without any input from the material investigation of the Helperzoom girders—all the material inputs are based on the provisions in RBK and RTD 1016-1:2020. One set of these simulations is developed without any safety format with mean material properties and is referred to as RBK—Mean xxxx, while the other uses a GRF safety format and is referred to as RBK—GRF xxxx, where "xxxx" stands for the shear span of the respective simulation in mm (refer to Table 1). The properties used for each of these material models are provided in Table 2. For brittle failures, like shear failure, the recommended value of the GRF (γ_0) is 1.40 and the results of the simulation are modified as follows

$$P_{GRF} = \frac{P_{Num}}{\gamma_0} \quad (1)$$

where P_{GRF} is the load predicted with the GRF safety format; P_{Num} is the output of the simulation; and γ_0 is the GRF.

Geometry of finite element model

All the numerical models are developed in the 2-D work environment of DIANA 10.2 (DIANA FEA BV 2017). The total girder length is taken as 11.70 m (38.39 ft) (simplification from the experiments) with a span length of 9.60 m (31.49 ft) (as used in the experiments). To assign the cross-sectional geometry, the spatial function is used as available in DIANA 10.2 (DIANA FEA BV 2017), which defines the variation in width along the height of the girder as a fraction of its maximum width. The geometry of the anchor block is included in the model to apply prestressing load without causing splitting cracks (refer to Fig. 2). However, the stubs of the intermediate diaphragms are neglected for this study as they are not located in the region of interest.

To simulate the loading and support plates, a linear elastic material model is used for the steel with an elastic modulus of 210 GPa (30,458 ksi). To avoid the concentration of stresses around these plates, an interface element with a vertical stiffness equal to the stiffness of the concrete is used between the steel and concrete. The horizontal stiffness of this interface is assumed to be 1000 times lower than the vertical stiffness to simulate low-friction supports. In all the simulations, the support plates are 200 x 200 x 100 mm (7.87 x 7.87 x 3.94 in.), and the loading plate is 300 x 300 x 100 mm (11.81 x 11.81 x 3.94 in.).

Table 1—Name and description of numerical models

Numerical model	Shear span, mm*	Prestress level, MPa	Material model
HPZ01—Num	2900	695	Experimental
HPZ02—Num	2900	725	Experimental
HPZ03—Num	4400	700	Experimental
HPZ04—Num	4400	780	Experimental
RBK—Mean 2900	2900	870	RBK—Mean
RBK—GRF 2900	2900	870	RBK—GRF
RBK—Mean 4400	4400	870	RBK—Mean
RBK—GRF 4400	4400	870	RBK—GRF

*Loaded span of girders is simplified from 2903 to 2900 mm (114.3 to 114.2 in.) in simulations.

Note: 1 mm = 0.04 in.; 1 MPa = 145 psi.

Table 2—Definition of material properties in nonlinear models

Material	Property	Unit	RBK—Mean	RBK—GRF*	Experimental
Concrete	Young's modulus	MPa	38,214	38,214	38,547
	Tensile strength	MPa	4.21	2.51	4.27
	Compressive strength	MPa	63.00	46.75	64.85
	Tensile fracture energy	N/mm	0.108	0.092	0.108
	Compressive fracture energy	N/mm	34	28.5	34
Mild steel	Young's modulus	MPa	210,000	210,000	200,000
	Yield strength	MPa	440	440	454
	Tensile strength	MPa	480	530	655
Prestressing steel	Young's modulus	MPa	195,000	195,000	185,000
	0.1% proof stress	MPa	1570	1635	1433
	Tensile strength	MPa	1843	1920	1824

*GRF properties are calculated by multiplying characteristic material properties with 0.85 for concrete, 1.1 for reinforcing steel, and 1.15 for prestressing steel following guidelines where characteristic parameters are derived from mean value using $f_{ck} = f_{cm} - 8$ and $f_{ctk} = 0.7 f_{ctm}$.

Note: 1 MPa = 145 psi.

The layout of the prestressing cable is determined using the construction drawings of the Helperzoom bridge girders, as shown in Fig. 1(c) and 3(a). The cables are modeled as embedded elements—that is, they do not have a mass of their own but add stiffness to their corresponding concrete element. In principle, they behave like truss elements. Furthermore, a perfect bond between concrete and tendons is assumed.

An anchor block and tapered part are present at the end of the girder, so that shear failure at the anchorage zone with prestressing loss is not expected. The prestressing losses are not explicitly modeled because a lower-bound value of the working prestress is used in the simulations.

As discussed earlier and shown in Fig. 1(a) and (b), the stirrups follow the shape of the bulb-T-girder profile, which is not permitted by modern design codes. In the experiment (Lantsoght et al. 2021), it is observed that the stirrups can still reach the yield stress. Therefore, these are modeled as embedded reinforcement with a perfect bond.

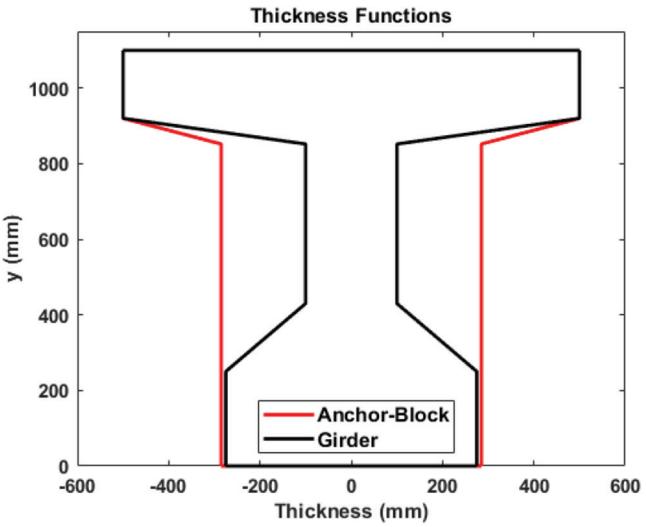

Fig. 2—Cross section of girder and anchor block in simulations. (Note: Dimensions in mm; 1 mm = 0.04 in.)

For HPZ01—Num and HPZ02—Num, the load is applied at 2900 mm (114 in.) from the left support, as shown in Fig. 3(a). For HPZ03—Num and HPZ04—Num, the load is applied at 4400 mm (173 in.) from the support.

During all the experiments, vertical external prestressing near the saw cut is used to avoid slipping of the prestressing steel. In particular, for the load location in HPZ03 and HPZ04, this vertical prestressing helps to avoid a shear failure outside the region of interest. In the numerical study, the same effect is achieved in HPZ03—Num and HPZ04—Num by doubling the number of stirrups outside the region of interest, as shown in Fig. 3(b). For HPZ01—Num and HPZ02—Num, this change in stirrup spacing is not applied. The rest of the reinforcement (including the prestressing tendon profile) is the same as in the tested specimens as shown in Fig. 1.

Material modeling

Three different material models are used in this study, as shown in Table 1. Table 2 gives the properties of each material model. Two material models are predictive, and hence do not require any input from material investigations on the girders. The experimental material model, however, uses measured material properties. The concrete compressive strength for the experimental material model is taken as 64.85 MPa (9406 psi), corresponding to the average tested cylinder compressive strength (Lantsoght et al. 2020). All other properties (tensile strength and fracture energies) are determined from the compressive strength as prescribed in RTD 1016-1:2020, with tensile strength and fracture energy determined as

$$f_{ctm} = 2.12\ln(1 + 0.1f_{cm}) \quad (2)$$

$$G_{Fk} = 0.7 \times 0.073 f_{cm}^{0.18} \quad (3)$$

The steel properties are also classified through experimental investigations. The mild steel is characterized as FeB400 with a mean yield strength of 440 MPa (64 ksi) and ductility class B ($f_t/f_y \geq 1.08$ and $\varepsilon_u > 5\%$). The prestressing steel is classified as QP170, having a mean yield strength

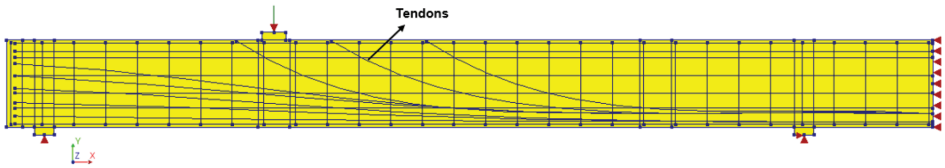

(a) Reinforcement, tendon layout and boundary conditions for HPZ01 – Num and HPZ02 – Num

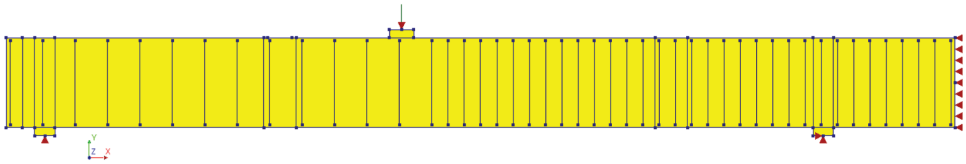

(b) Stirrup configuration for HPZ03 – Num and HPZ04 – Num

Fig. 3—(a) Finite element models for HPZ01—Num and HPZ02—Num; and (b) stirrup configuration for HPZ03—Num and HPZ04—Num.

of 1433 MPa (208 ksi) and a tensile strength of 1824 MPa (265 ksi). The prestressing losses are not explicitly modeled because a lower-bound value of working prestress is used in the simulations.

The models with the experimentally determined material properties are referred to as HPZ0x—Num, where "x" is 1 to 4. These models do not use any safety format; their aim is to reproduce the experiment.

Following the RTD 1016-1:2020 guidelines, all simulations use the Hordijk softening curve (Hordijk 1991) for concrete in tension and a parabolic stress-strain relationship (Feenstra 1993) for concrete in compression. A smeared crack approach (Rashid 1968) is used with a rotating crack model. Research has shown that the rotating crack model is suitable for predicting the capacities of members failing in shear (Rots et al. 1985; Rots and Blaauwendraad 1989).

Furthermore, because a large post-yielding ductility was observed in the experiments, the rotating crack model is preferred over the fixed crack model, because the fixed crack model resists the rotation of the shear crack, leading to premature failure and underprediction of the capacity (de Putter et al. 2022). A von Mises plasticity model with isotropic hardening is used for both mild and prestressing steel. A perfect bond between the concrete and steel is assumed by using the embedded reinforcement option.

RBK suggests a working prestress level in the bridge girders following their year of construction. For the Helperzoom girders, this working prestress level is 870 MPa (126 ksi). Therefore, in simulations with the RBK—Mean and RBK—GRF material models, this value is used. However, the laboratory experiments combined with the sectional analysis indicated lower levels of prestressing in the girders: 695 MPa (101 ksi) for HPZ01, 725 MPa (105 ksi) for HPZ02, 700 MPa (102 ksi) for HPZ03, and 780 MPa (113 ksi) for HPZ04. As such, for HPZ01—Num, HPZ02—Num, HPZ03—Num, and HPZ04—Num, these respective values for the working prestress level are used.

Finite element analysis

The girders are modeled using eight-node (quadrilateral) regular plane stress elements with quadratic interpolation. The mesh size of 100 mm (3.94 in.) is chosen such that there are six elements in the web of the girder assuming a web height of 600 mm (23.62 in.). For all the numerical models, the energy norm is used as a convergence criterion with a tolerance of 0.001 to ensure the stability of the simulations. All the analyses show acceptable convergence behavior and are allowed to run until the relative energy error does not exceed 0.01.

A phased analysis is performed in which the prestressing and self-weight are applied in the first phase, followed by the application of deformation at the loading point with a load step of 0.5 mm (0.0197 in.) to represent the load applied during the experiment.

The post-tensioning is applied on the full girder at the time of construction, and the tendons are cut in half before transportation to the laboratory. To simulate this situation in the numerical model, the symmetry condition (refer to Fig. 3) is used in the first phase of the analysis. In the second phase, this symmetry boundary condition is removed.

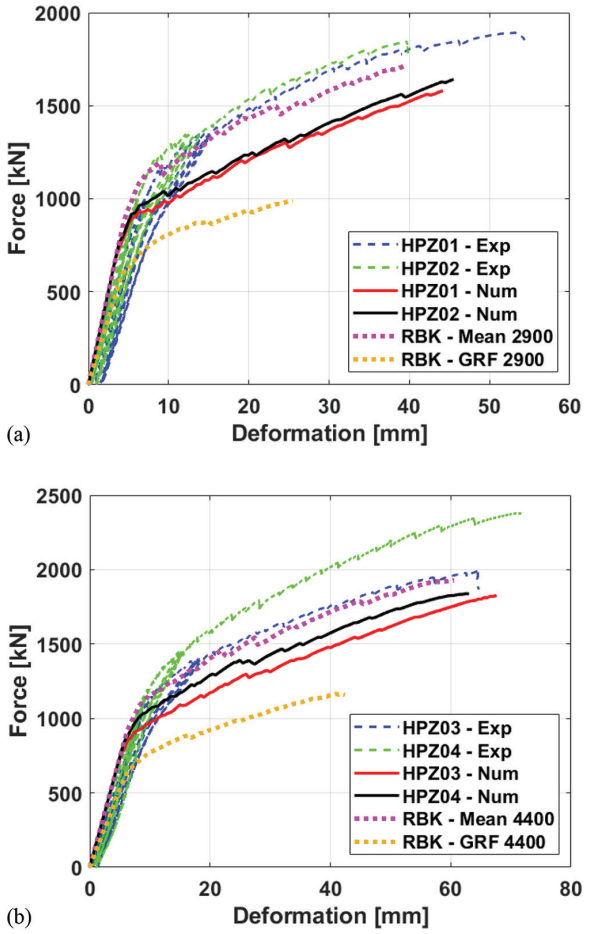

Fig. 4—Experimental and numerical load-deformation response of girders loaded at: (a) 2900 mm; and (b) 4400 mm. (Note: 1 mm = 0.04 in.; 1 kN = 0.225 kip.)

COMPARISON BETWEEN FINITE ELEMENT ANALYSIS AND EXPERIMENTS

Comparison between shear behavior in experiments and numerical models

To assess the accuracy of the numerical model, the numerical and experimental load-deformation behavior (Fig. 4) and crack pattern (Fig. 5 to 7) are compared. As discussed previously, the GRF safety format is for the determination of the load-carrying capacity at the ultimate limit state, but for representation, the entire load-deformation response of RBK—GRF 2900 and RBK—GRF 4400 is plotted in Fig. 4 after adjustment with the GRF, as described in Eq. (1). In Fig. 4, HPZ0x—Exp refers to the experimentally observed load-deflection behavior of the girders, where "x" ranges from 1 to 4.

As seen in Fig. 4, all the simulations have an initial global stiffness in good accordance with the experiments. The loading scheme adapted for the test included cycles of loading and unloading, which resulted in a gradual decrease in the stiffness of the girder. As this loading history is not simulated in the models, the stiffness of the model should be compared with the first loading of the sample.

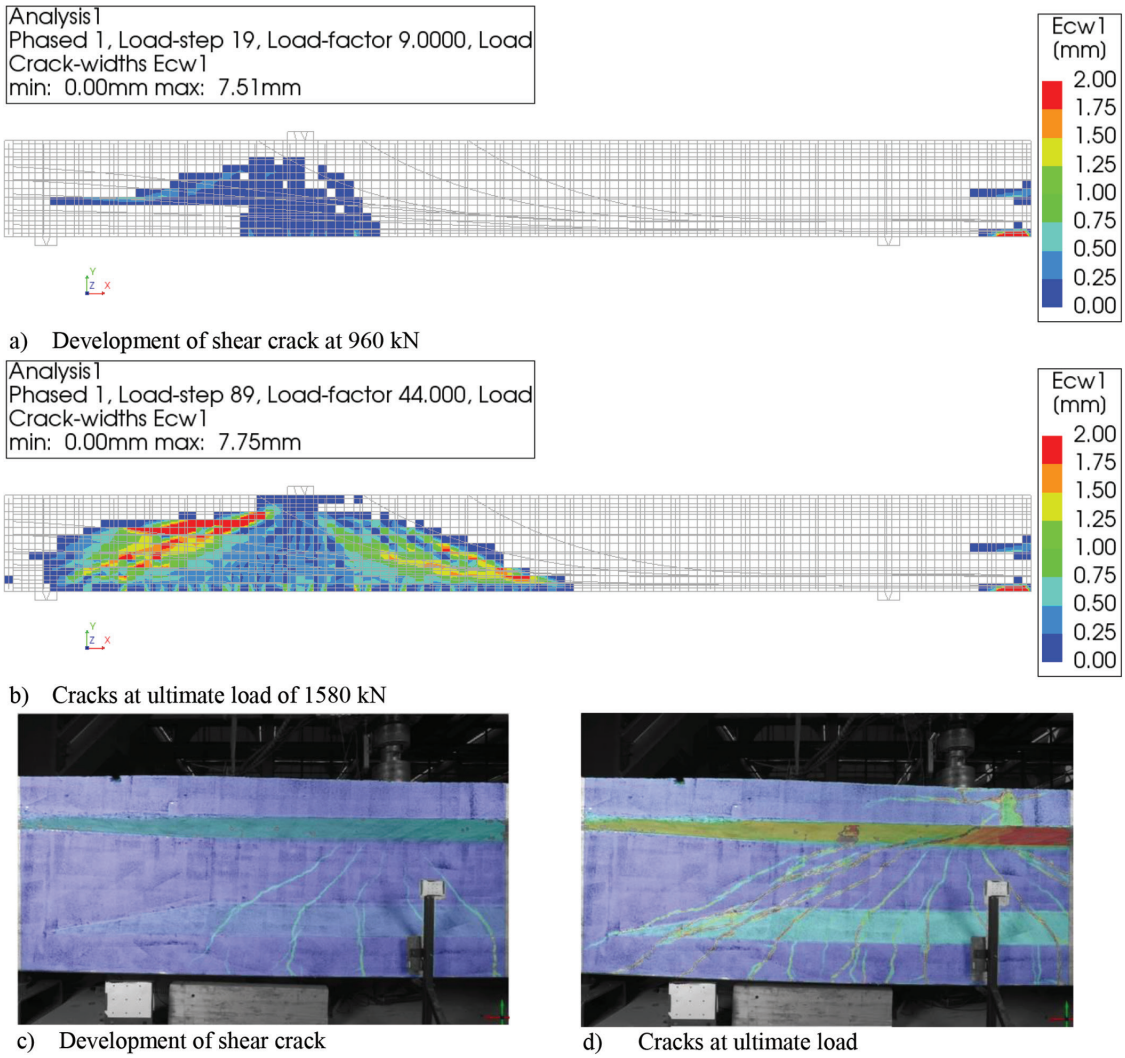

Fig. 5—Numerical crack pattern at: (a) shear crack development; and (b) ultimate load of HPZ01—Num; and crack pattern observed with digital image correlation (DIC) at: (c) development of shear crack; and (d) ultimate load of HPZ01. (Note: 1 mm = 0.04 in.; 1 kN = 0.225 kip.)

All the experiments showed an increase in the load-carrying capacity after the development of the shear crack because of the contribution from the non-code-compliant stirrups. The same is also observed in all the numerical simulations, showing that the modeling choices used can simulate the stirrup contribution appropriately.

From Fig. 4(a), it can be seen that RBK—Mean 2900 is able to predict the behavior of the girder in good accordance with the experiments. This is because RBK predicted the same concrete class as observed in the experimental material investigations and the assumed working prestress is higher than derived from the experiments. When the actual working prestress is used in HPZ01—Num and HPZ02—Num, the shear crack develops at a lower load level because the strength of the critical section is lower; however, the final capacity is not significantly affected. The predicted capacity of RBK—GRF 2900 is approximately 1.8 times lower when compared to RBK—Mean 2900 and the experiments because it takes into account the potential uncertainties in modeling and material.

HPZ01—Num and HPZ02—Num show similar cracking behavior as the only difference between these two is a slightly different prestress level (695 MPa [101 ksi] for HPZ01—Num and 725 MPa [105 ksi] for HPZ02—Num). Therefore, only the crack pattern of HPZ01—Num is shown and compared with the experimental observations, which are also quite similar for the two experiments, HPZ01—Exp and HPZ02—Exp.

Comparing the numerical and experimental crack patterns (Fig. 5), some differences in the cracks are observed at the development of the shear crack and at the ultimate load. Most notably, the angle of the shear crack in the simulations is less than in the corresponding experiment—an effect of the rotating crack model used in the simulations (de Putter et al. 2022). However, the numerical simulations show the same sequence of cracking as observed in the experiments—that is, flexure, flexure-shear, shear-tension, and then failure. All the simulations with load at 2900 mm (114 in.) show that concrete crushing drives the failure, as also observed in the experiments. In the numerical simulation, the cracks observed at the symmetry line result from the removal of the

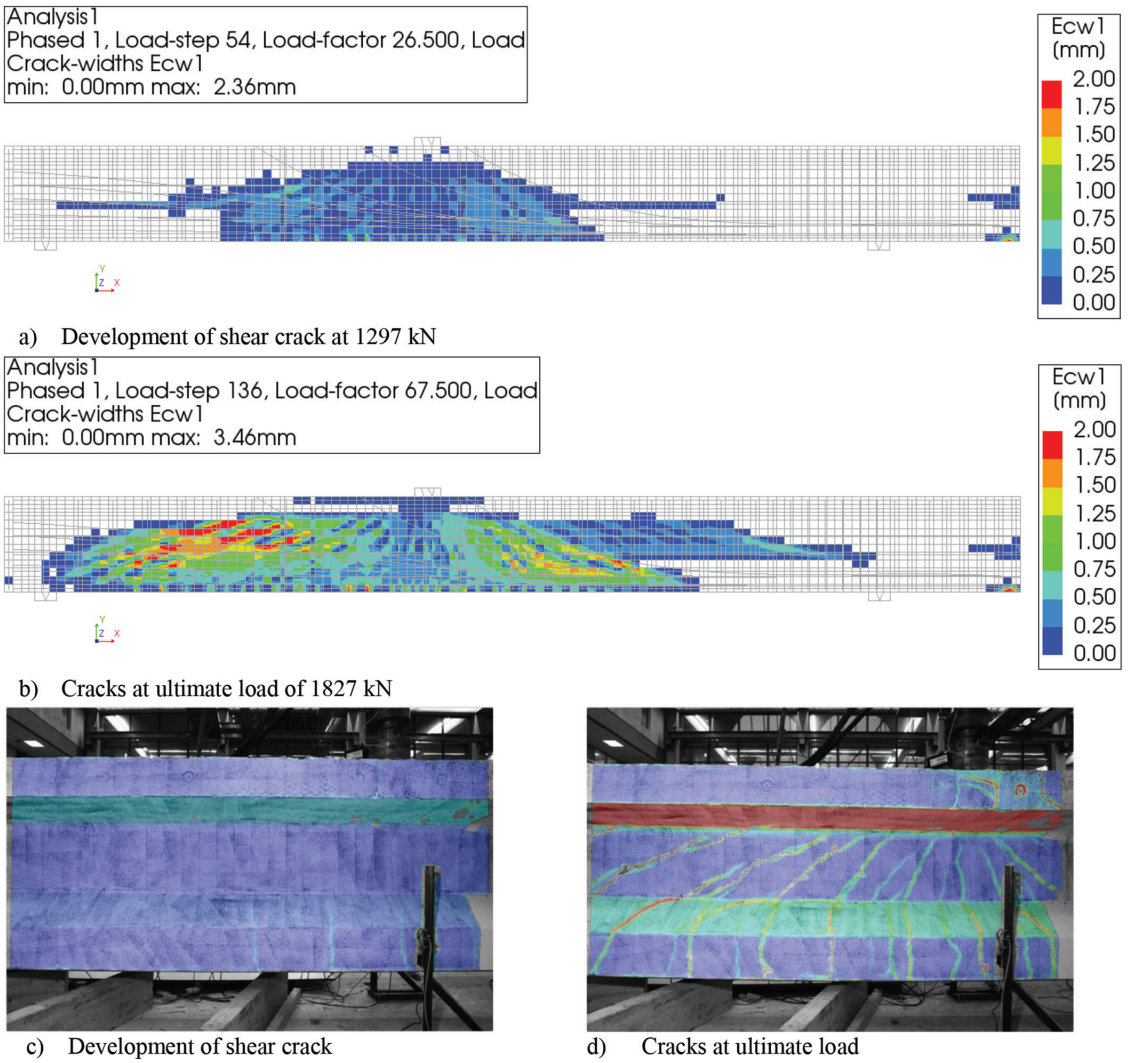

Fig. 6—Numerical crack pattern at: (a) shear crack development; and (b) ultimate load of HPZ03—Num; and crack pattern observed with DIC at: (c) development of shear crack; and (d) ultimate load of HPZ03. (Note: 1 mm = 0.04 in.; 1 kN = 0.225 kip.)

symmetry boundary condition at the beginning of the second phase of the analysis and can be ignored in this study as these cracks are not in the shear span.

A similar comparison is made between the girders loaded at 4400 mm (173 in.). HPZ04—Exp shows a different stiffness after the development of the shear crack than HPZ03—Exp. Similar trends are observed in terms of the predicted response for the RBK—Mean 4400 and RBK—GRF 4400 models when compared to the simulations with the experimental material models (HPZ03—Num and HPZ04—Num) and experiments. A comparison of the numerical and experimental crack patterns again shows a higher rotation of the shear crack for both HPZ03 (Fig. 6) and HPZ04 (Fig. 7). The sequence of cracking in the numerical simulations is in the same order as in the experiments.

Because the goal of the study is not to perfectly replicate the experimental observations but to check the robustness of the RTD guidelines when applied to a complex situation, such as the Helperzoom girders, the resulting crack pattern is acceptable for the purpose.

Overview of comparison of results

Table 3 gives an overview of the important points on the load-deflection diagram from the experiments and numerical analyses. The points of interest are the development of the first flexural crack, the development of the flexure-shear crack, the development of the shear-tension crack, and the ultimate load. For reference, the working prestress in each experiment σ_{pw}, derived from sectional analysis (Lantsoght et al. 2021) or from the RBK provisions, is included in Table 3 as well. To evaluate these results, Table 4 reports the ratios of the tested to numerically predicted values for these four points of interest, along with the average (AVG), standard deviation (STD), and coefficient of variation (COV). These values are not intended to establish the accuracy of finite element analysis statistically but only to compare the observed experimental and numerical responses of the girders. First, the simulations with the experimentally observed material properties are compared, and then the RBK—Mean and RBK—GRF models are discussed.

For flexural and flexure-shear cracking loads, the simulations with the experimentally observed material models

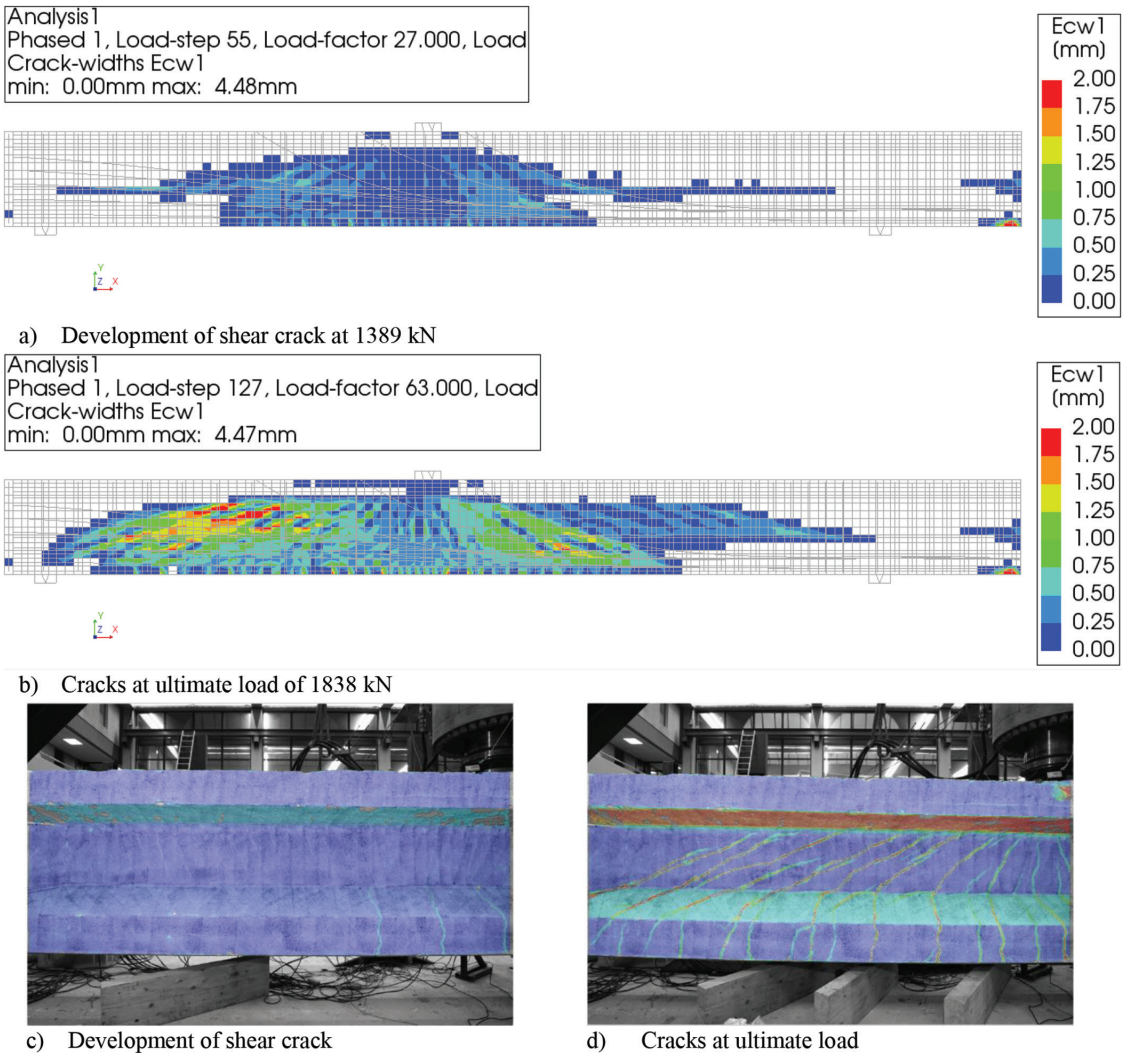

Fig. 7—Numerical crack pattern at: (a) shear crack development; and (b) ultimate load of HPZ04—Num; and crack pattern observed with DIC at: (c) development of shear crack; and (d) ultimate load of HPZ04. (Note: 1 mm = 0.04 in.; 1 kN = 0.225 kip.)

Table 3—Comparison of cracking loads of all girders with calculated prestress level

			Numerical results					Experimental results				
	σ_{pw}, MPa	Shear span, mm	F_{crack}, kN	$F_{flexure\text{-}shear}$, kN	$F_{shear\text{-}tension}$, kN	$F_{ultimate}$, kN	FM	F_{crack}, kN	$F_{flexure\text{-}shear}$, kN	$F_{shear\text{-}tension}$, kN	$F_{ultimate}$, kN	FM
HPZ01—Num	695	2900	674	928	960	1580	SC	965	1344	1480	1893	SC
HPZ02—Num	725	2900	675	979	1040	1642	SC	1001	1299	1350	1849	SC
HPZ03—Num	700	4400	717	927	1297	1827	SC	1025	1250	1600	1990	CC
HPZ04—Num	780	4400	790	1039	1389	1838	SC	1100	1450	1750	2380	CF
RBK—Mean 2900	870	2900	861	1177	1130	1717	SC	—	—	—	—	—
RBK—GRF 2900	870	2900	548	723	610	986	ST	—	—	—	—	—
RBK—Mean 4400	870	4400	858	1156	1543	1928	SC	—	—	—	—	—
RBK—GRF 4400	870	4400	558	777	870	1158	SC	—	—	—	—	—

Note: FM is failure mode; SC is shear-compression failure; ST is shear-tension; CC is crushing of concrete in compression zone; and CF is crushing of concrete struts in web.
1 MPa = 145 psi; 1 kN = 0.225 kip.

(HPZ01—Num to HPZ04—Num) and prestressing forces are found to be conservative with respect to the experiments with the average tested-to-predicted ratios of 1.43 and 1.38, respectively. The effect of load position is found to be limited on both the tested-to-predicted ratio of flexure and flexure-shear cracking given the limited variation in tested-to-predicted ratios of beams loaded at 2900 and 4400 mm (114 and 173 in.). For the shear-tension cracking

Table 4—Statistical comparison between experimental and numerical results

	Tested-to-predicted ratios											
	Experimental material model (HPZ0x—Num)				RBK—mean model (RBK—Mean xxxx)				RBK—GRF model (RBK—GRF xxxx)			
Girder number	F	FS	ST	U	F	FS	ST	U	F	FS	ST	U
HPZ01	1.43	1.45	1.54	1.20	1.12	1.14	1.31	1.10	1.76	1.86	2.43	1.92
HPZ02	1.48	1.33	1.30	1.13	1.16	1.10	1.19	1.08	1.83	1.80	2.21	1.88
HPZ03	1.43	1.35	1.23	1.09	1.19	1.08	1.04	1.03	1.84	1.61	1.84	1.72
HPZ04	1.39	1.40	1.26	1.29	1.28	1.25	1.13	1.23	1.97	1.87	2.01	2.06
AVG	1.43	1.38	1.33	1.18	1.19	1.15	1.17	1.11	1.85	1.78	2.12	1.89
STD	0.032	0.047	0.122	0.078	0.059	0.067	0.099	0.075	0.076	0.104	0.220	0.120
COV %	2.2	3.4	9.2	6.7	5.0	5.8	8.5	6.8	4.1	5.8	10.4	6.4

Note: F is flexure; FS is flexure-shear; ST is shear-tension; U is ultimate failure; AVG is average; STD is standard deviation; and COV is coefficient of variation.

load, the models are conservative, but more so for the load at 2900 mm (114 in.) than for the load at 4400 mm (173 in.). For the ultimate load, the numerical predictions are also on the conservative side (average tested-to-predicted ratio = 1.18). HPZ03—Num is able to predict the ultimate load in good accordance with the experiment, but HPZ04—Num fails at a lower load than experimentally observed. In the experiment of HPZ04, the failure mode is crushing of the concrete compression field in the web of the girder, whereas the numerically observed failure mode of HPZ04—Num is the crushing of the concrete at the point of application of the load.

The RBK—Mean approach results in conservative predictions for all the points of interest on the load-deformation diagram. The values predicted with the RBK—Mean approach are less conservative for all the points of interest when compared to the numerical simulations with the experimentally observed material properties. The RBK—Mean approach provides sufficient accuracy to model the behavior of girders, but in practice, additional safety factors are required to ensure safety, as represented by the RBK—GRF method. As such, the RBK—Mean material model can only be used when comparing the results of the numerical simulations with the experiments and not for the assessment of existing concrete structures.

The tested-to-predicted ratios for the simulations with the RBK—GRF approach are higher due to the explicit consideration of numerical and material factors. They provide a sufficient margin of safety from the actual capacity, which is comparable to the analytical predictions obtained using design codes (Park et al. 2021).

Overall, the results in Tables 3 and 4 show that the numerical models provide a conservative estimate of the behavior of post-tensioned bridge girders failing in shear. Although the failure modes of HPZ03—Num and HPZ04—Num do not correspond to the experimentally observed failure mode, the simulations reflect the crucial elements of the experiment—that is, the ability of the girder to carry load after inclined cracking, and the overall load-deflection behavior of the girder (refer to Fig. 4). The recommendations from the Dutch guidelines, RTD 1016-1:2020 and RTD 1006:2013, and the resulting modeling approach can thus be used for the assessment of bridge girders in slab-between-girder bridges.

ADDITIONAL PARAMETER STUDIES

Justification of parameter studies

The original experimental plan included eight girders. However, during the execution phase, four girders were damaged during sawing. Consequently, only four girders were available for testing. Although these tests provided valuable data to understand the shear capacity of the existing prestressed girders, they also left several questions that may further influence the preliminary conclusions obtained from the experimental program.

As only two loading positions are tested, it is not clear if these are the critical loading positions. Because of the complex geometry, analytical models do not guarantee an accurate prediction either. Thus, further study on the influence of the loading position on the shear capacity of the girders is necessary.

From the experimental program, it turns out that the residual prestress level of the bridge girders may be lower than the value expected based on RBK. It is therefore important to assess the influence of the residual prestress level on the capacity of the girders. The conclusion may affect the assessment procedure of the existing prestressed girders.

By comparing with the experimental results, this study's numerical models are shown to be able to simulate the behavior of the girders with sufficient accuracy. These models provide an opportunity to extend the experimental program with additional numerical simulations to study the influence of the position of the load and the prestress level. For these parameter studies, the experimental material model is used, and five new models are developed. The results of HPZ01—Num and HPZ03—Num are included in the parameter study of the prestress level. A description of all the models of the parameter studies is provided in Table 5.

Influence of position of load

To study the effect of load position on the behavior of the girders, a constant prestress of 870 MPa (126 ksi) is assumed, and the load is applied at 1400, 2900, and 4400 mm (55, 114,

and 173 in.) from the support (Table 5). The influence of the load position is studied by comparing the load-deflection response, flexural cracking load, flexure-shear cracking load, shear-tension cracking load, and ultimate load, as depicted in Fig. 8.

From Fig. 8(a), it can be observed that the initial global stiffness increases as the distance between the support and the load is reduced. The larger stiffness results from the lower bending deformations due to the shorter shear span. Furthermore, with a shorter shear span, the anchor block also contributes to this increase in initial global stiffness due to its larger cross-sectional dimensions than the girder, as shown in Fig. 2. The deformation capacity of the girders decreases as the shear span is reduced because higher values of sectional shear are generated at the same load but the bending moments and flexural deformations are lower. Exp-870-2900 and Exp-870-4400 show sufficient deformation capacity after the development of the shear crack due to the contribution of stirrups, as also observed in the experiments. Compression drives the ultimate failure. However, the response of the girder loaded at 1400 mm (55 in.)—that is, Exp-870-1400, is rather brittle and the failure mode is shear-tension.

Figure 8(b) shows that as the load moves further away from the support, the flexural and flexure-shear cracking load decrease owing to the larger shear span and thus larger bending moment for the same applied load. The effect is not pronounced for Exp-870-2900 and Exp-870-4400 because of the additional tendons resulting in higher compressive forces at the bottom fibers. There is also a direct correlation between the distance from the support and the load for the development of the shear-tension crack. The difference is more pronounced for the shear spans of 2900 and 4400 mm (114 and 173 in.) and can be attributed to the higher precompression of the section due to additional tendons, as shown in Fig. 1(c). The order of cracking events also changes with load location, as in Exp-870-2900 and Exp-870-4400, flexural cracking is observed before shear-tension cracking, while for Exp-870-1400, the flexural cracks develop after the formation of the shear-tension crack, as the cracking moment is reached for a higher applied load. The ultimate failure load is the largest for the shortest shear span due to the significant direct transfer of the load from its point of application to the support.

From this study, it can be concluded that the load position influences the load-deformation response of prestressed concrete girders, especially in terms of the initial stiffness, order of cracking events, and failure mode. The load location also determines the number of active tendons in the shear span, which further influences the girder response. The shorter shear spans result in a stiffer and more brittle response as the girder experiences higher shear stresses and lower bending moments. For shorter shear spans, direct transfer of the load to the support becomes an additional mechanism, significantly increasing the ultimate capacity. For the studied sample, the weakest location is at 2900 mm (114 in.) from the support, which is in accordance with the initial calculations (Roosen 2017) following the current Dutch assessment practices to determine the shear-critical load position of existing post-tensioned girders.

Table 5—Description of numerical models for load position and working prestress level sensitivity analysis

Parameter study	Model ID	Material model	Working prestress level, MPa	Shear span, mm
Position of load	Exp-870-1400	Experimental	870	1400
	Exp-870-2900	Experimental	870	2900
	Exp-870-4400	Experimental	870	4400
Prestress level	Exp-600-2900	Experimental	600	2900
	HPZ01—Num	Experimental	695	2900
	Exp-870-2900	Experimental	870	2900
	Exp-600-4400	Experimental	600	4400
	HPZ03—Num	Experimental	700	4400
	Exp-870-4400	Experimental	870	4400

Note: 1 mm = 0.04 in.; 1 MPa = 145 psi.

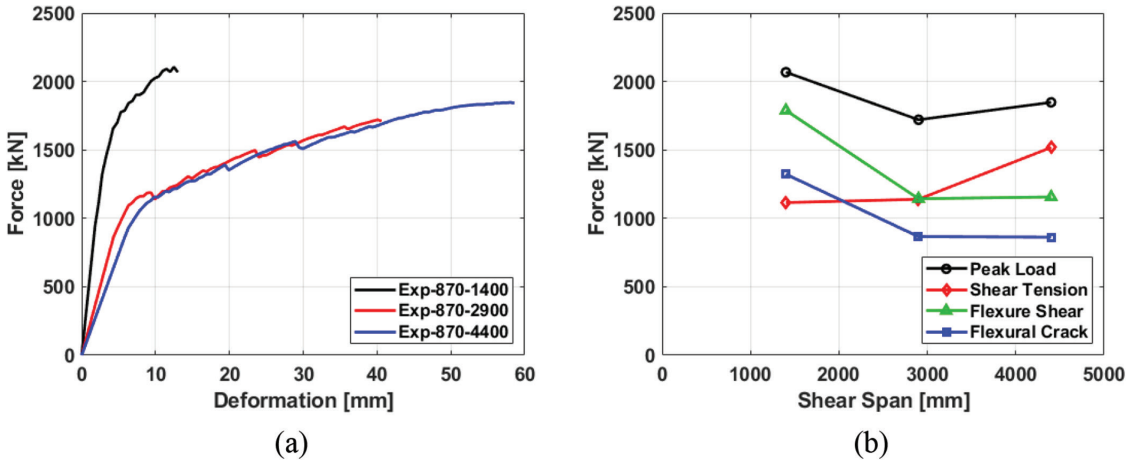

Fig. 8—Influence of load position on: (a) load-deformation behavior; and (b) critical loads. (Note: 1 kN = 0.225 kip; 1 mm = 0.04 in.)

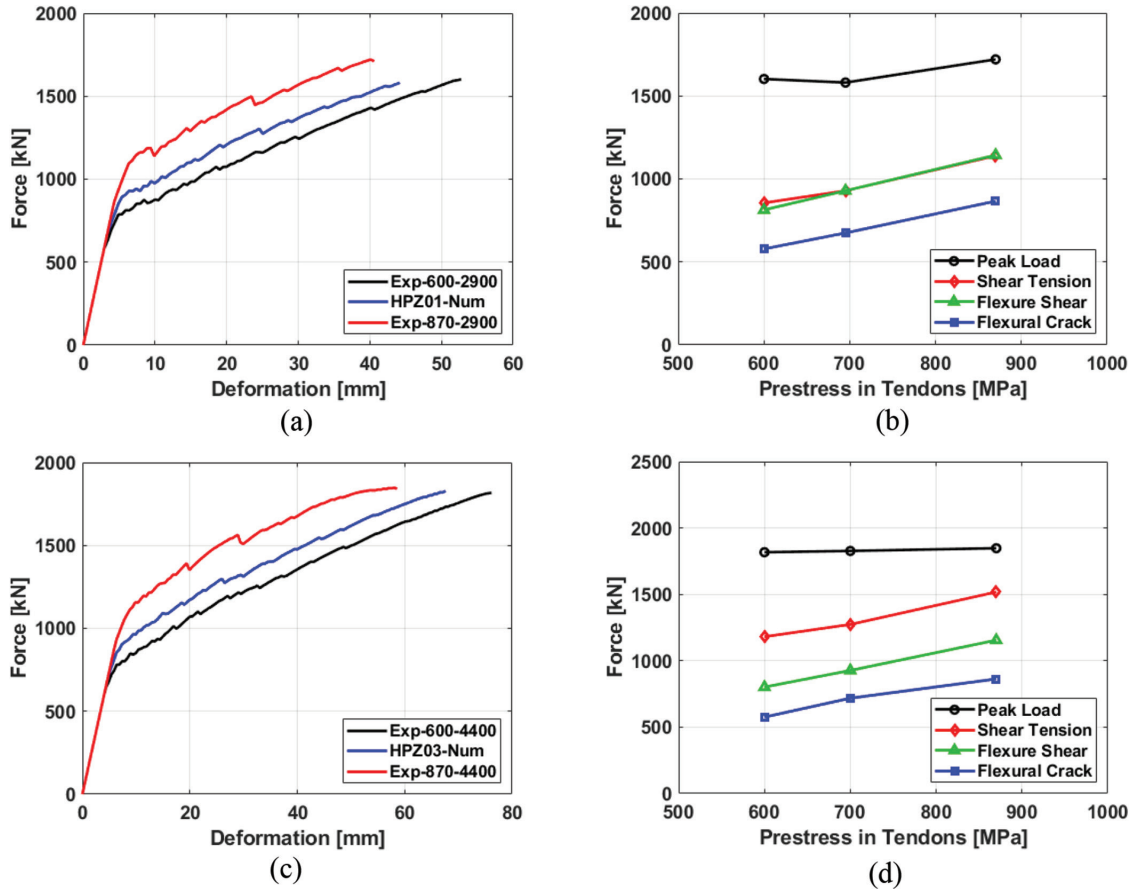

Fig. 9—Influence of prestress level on: (a) load-deformation behavior; and (b) critical loads for load at 2900 mm (114 in.); and (c) load-deformation behavior; and (d) critical loads for load at 4400 mm (173 in.). (Note: 1 kN = 0.225 kip; 1 mm = 0.04 in.; 1 MPa = 145 psi.)

Influence of prestress level

If the ultimate capacity of the structural members is governed by flexural failure, then the effect of the level of prestressing on the ultimate load-carrying capacity of the member is limited. However, for the case of the investigated girder, the prestress level is quite important because it determines the load for the development of cracks and the distribution of principal stresses in the structure. Accurate prediction of the working prestress level in existing bridge girders still poses a challenge to bridge owners, making it essential to investigate the influence of varying assumptions for working prestress on the response of prestressed concrete girders, especially when shear is critical. This parameter analysis is therefore aimed at getting insight into the effect of varying the level of prestressing on the flexural cracking, flexure-shear cracking, shear-tension cracking, peak load, and failure mode of prestressed concrete girders.

The effect of the prestress level is studied for both load locations at 2900 and 4400 mm (114 and 173 in.). The prestressing value varies from 600 to 870 MPa (87 to 126 ksi) (refer to Table 5). The results are plotted in Fig. 9.

For both load locations, prestressing shows a similar effect in terms of the change in the load-deformation response. The initial and final stiffness of the girders remain unaffected (refer to Fig. 9(a) and (c)) as this depends on the cross-sectional properties of the girder and not the prestressing forces. Increasing the prestress level delays the formation of the first flexural crack due to higher compressive forces at the bottom of the girder before applying the load. This effect is independent of the load location as an increase in flexural cracking load of approximately 50% is observed for both positions when the prestressing is increased from 600 to 870 MPa (87 to 126 ksi)—refer to Fig. 9(b) and (d). Increasing the prestress level also causes a delay in the development of the flexure-shear and shear-tension crack as higher precompression forces exist in the critical cross section prior to the application of the load. However, prestressing seems to have little effect on the ultimate load-carrying capacity of the girders for both the loading positions—for the load at 2900 mm (114 in.) and 4400 mm (173 in.), the capacity is increased by 7% and 2%, respectively, when the prestressing is increased from 600 to 870 MPa (87 to 126 ksi). All the girders fail in shear-compression, so the ultimate capacity is governed by the compressive strength of concrete. However, the deformation capacity of the girders reduces significantly as the prestressing forces increase. A larger prestress delays the onset of flexural cracking, leading to fewer cracks and lower deformations at the ultimate load.

From this study, it can be concluded that increasing prestressing increases the cracking moment, flexure-shear, and shear-tension load of girders, but the effect on the ultimate load-carrying capacity is limited when a shear-compression failure is observed. However, the deformation capacity

of the girder reduces with an increase in prestressing forces, making the girders more brittle.

DISCUSSION

The first observation from this study is that following the Dutch Guidelines for Nonlinear Finite Element Analysis leads to the good performance of the numerical models. The recommended values for the material properties are updated in this study with the experimentally determined values, but the material models are kept as recommended by the guidelines. The models using the GRF safety format provide a safe estimate of the experimental behavior. From this study, it is found that the guidelines work well for the prediction of the behavior of complex bridge girders with a changing cross section and draped tendon layout that have been in service for decades.

The second observation of this work is that it confirms the critical position of these girders as first estimated based on a shear crack angle of 30 degrees between the load and the position of the beginning of the regular thin-webbed cross section (after the anchorage block and tapered transition part). Because the provided stirrups are less than the minimum required amount and follow the shape of the girder, their capacity cannot be included in regular assessment calculations. As a result, assessment calculations indicate that the critical failure mode for these girders is shear-tension. With the experiments it is observed that the stirrups are activated and that the critical failure mode for the studied positions is shear-compression or crushing of the concrete in the web.

In terms of the influence of the prestress level, it is observed that this parameter mainly influences the flexural cracking load and the shear cracking load. The ultimate load is less influenced by this parameter. However, for bridge girders, the serviceability requirements are an important step in design, as the design is based on the requirement of no or limited tensile stresses in the cross section. When cracks appear, the behavior of the girder changes significantly and the serviceability requirements are violated. For this reason, estimating the prestress level in existing girder bridges is important for assessment, and nondestructive techniques for this purpose need to be explored further.

Guidelines for the use of nonlinear finite element models are a good tool for the implementation in practice of such models. In the past, nonlinear finite element models were sometimes criticized because of the large range of outcomes in prediction competitions by users who predicted failure loads and behavior with nonlinear finite element models (Collins et al. 2015; de Boer et al. 2018; Jaeger and Marti 2009). For this reason, guidelines for the use of nonlinear finite element models are valuable, as they reduce the number of decisions the user makes and help achieve more uniform outcomes. As such, the outcomes of this research pave the way toward broader implementation of nonlinear finite element models in the assessment of existing bridges in the Netherlands as well as internationally.

SUMMARY AND CONCLUSIONS

This paper presents the numerical simulations and associated parameter studies of post-tensioned concrete bridge girders taken from the Helperzoom bridge in the Netherlands and tested to shear failure in the laboratory. The numerical study is carried out to validate the Dutch Guidelines for Nonlinear Finite Element Analysis of Concrete Structures on large-sized girders with a realistic geometry (including anchor block and tapered part of the cross section) using draped tendons, to gain a deeper understanding of the shear-carrying behavior in the experiment, and to extend the test results with parameter studies.

To validate the Dutch guidelines, three sets of models are developed: a set used for assessment, including a global resistance factor (GRF) safety format, a set based on assumed average material properties based on the Dutch Guidelines for the Assessment of Existing Bridges (RBK), and a set updated with measured material properties in the laboratory. From these analyses, it is found that both the models with assumed and measured material properties perform well in replicating the experimental observations.

Finally, the insights of the experiments are extended with parameter studies to further study the influence of the position of the load and the prestress level. With regard to the position of the load, the estimated critical position for shear failure is confirmed by the numerical models and can thus be used for the assessment of existing girder bridges. With regard to the prestress level, it was found that the value mostly influences the flexural cracking and shear cracking loads. Because the flexural cracking load should not be exceeded for the performance of prestressed bridge girders, better nondestructive testing methods to determine this value are necessary.

Finally, the numerical models indicated a shear-compression failure for all modeled load positions, and that an abrupt shear-tension failure, which is identified in preliminary assessments as the governing failure mode for these types of bridge girders, is not the governing failure mode. Thanks to the activation of the non-code-compliant stirrups in the experiments and the perfect bond assumption between the reinforcing bar and concrete in the numerical models, more load can be carried after the initial flexure-shear or shear-tension cracking.

AUTHOR BIOS

Shozab Mustafa *is a PhD Candidate at Delft University of Technology, Delft, the Netherlands. He received his BSc in civil engineering from the National University of Sciences and Technology (NUST), Islamabad, Pakistan, in 2016, and his MSc from Delft University of Technology in 2019. His research interests include the characterization of concrete-concrete interfaces and modeling of concrete structures.*

ACI member **Eva O. L. Lantsoght** *is a Full Professor at the Universidad San Francisco de Quito, Quito, Ecuador, and an Assistant Professor at Delft University of Technology. She is Secretary of Joint ACI-ASCE Committee 421, Design of Reinforced Concrete Slabs, Vice Chair of Joint ACI-ASCE Subcommittee 445-E, Shear & Torsion-Torsion; and a member of ACI Committees 342, Evaluation of Concrete Bridges and Bridge Elements, and 437, Strength Evaluation of Existing Concrete Structures; Joint ACI-ASCE Committee 445, Shear and Torsion; and Joint ACI-ASCE Subcommittee 445-D, Shear & Torsion-Shear Databases.*

Yuguang Yang *is an Assistant Professor at Delft University of Technology. He received his BS in civil engineering from Shanghai Jiao Tong University,*

Shanghai, China, in 2005, and his MS and PhD in civil engineering from Delft University of Technology in 2007 and 2014, respectively. His research interests include the shear strength of reinforced concrete members, assessment of existing structures, and measurement techniques.

Henk Sliedrecht *is a Senior Consultant at Rijkswaterstaat, Ministry of Infrastructure and Water Management, Utrecht, the Netherlands. He received his MSc from Delft University of Technology. His research interests include the assessment of existing concrete bridges—in particular, methods of analysis and standards for structural safety.*

ACKNOWLEDGMENTS

The authors wish to express their gratitude and sincere appreciation to the Dutch Ministry of Infrastructure and the Environment (Rijkswaterstaat) for financing this research work. The authors are deeply indebted to their colleague A. Bosman for his work in the laboratory, development of the method to handle the girders, and design of the test setup. Thanks to J. Pawlowicz for his work in the laboratory and for managing the material testing. The authors express many thanks to their colleague M. Roosen for the preparatory calculations, to R. Braam and C. van der Veen for starting this research project and for their invaluable advice during the preparation and testing stages of this series of experiments, to former MSc thesis students N. Jayananda and J. Migalski for their prediction calculations, to PhD students G. Zarate and F. Zhang for their work in the laboratory and analysis through advanced measurement techniques, and to postdoctoral researcher M. K. Park for his sectional analysis of the beams.

NOTATION

F_{crack}	=	load at first flexural crack
$F_{flexure\text{-}shear}$	=	load at flexure-shear cracking
$F_{shear\text{-}tension}$	=	load at shear-tension cracking
$F_{ultimate}$	=	ultimate load capacity
f_{ck}	=	characteristic concrete compressive strength
f_{cm}	=	mean cylinder compressive strength of concrete
f_{ctk}	=	characteristic concrete tensile strength
f_{ctm}	=	mean tensile strength of concrete
f_t	=	tensile strength of reinforcement
f_y	=	yield strength of reinforcement
G_{Fk}	=	characteristic tensile fracture energy
h	=	height of cross section
L	=	span length
P_{GRF}	=	numerical ultimate load with GRF safety format
P_{Num}	=	numerical ultimate load
ε_u	=	ultimate strain of reinforcement
γ_0	=	global resistance factor for GRF safety format
σ_{pw}	=	working prestress level in girder

REFERENCES

Belletti, B.; Damoni, C.; den Uijl, J. A.; Hendriks, M. A. N.; and Walraven, J. C., 2013a, "Shear Resistance Evaluation of Prestressed Concrete Bridge Beams: *fib* Model Code 2010 Guidelines for Level IV Approximations," *Structural Concrete*, V. 14, No. 3, Sept., pp. 242-249. doi: 10.1002/suco.201200046

Belletti, B.; Damoni, C.; Hendriks, M. A. N.; and den Uijl, J. A., 2013b, "Nonlinear Finite Element Analyses of Reinforced Concrete Slabs: Comparison of Safety Formats," *VIII International Conference on Fracture Mechanics of Concrete and Concrete Structures (FraMCoS-8)*, J. G. M. Van Mier, G. Ruiz, C. Andrade, R. C. Yu, and X. X. Zhang, eds., 12 pp.

Bentz, E. C., 2000, "Sectional Analysis of Reinforced Concrete Members," PhD thesis, Department of Civil Engineering, University of Toronto, Toronto, ON, Canada.

Blomfors, M.; Engen, M.; and Plos, M., 2016, "Evaluation of Safety Formats for Non-Linear Finite Element Analyses of Statically Indeterminate Concrete Structures Subjected to Different Load Paths," *Structural Concrete*, V. 17, No. 1, Mar., pp. 44-51. doi: 10.1002/suco.201500059

Collins, M. P.; Bentz, E. C.; Quach, P. T.; and Proestos, G. T., 2015, "The Challenge of Predicting the Shear Strength of Very Thick Slabs," *Concrete International*, V. 37, No. 11, Nov., pp. 29-37.

de Boer, A.; Hendriks, M. A. N.; den Uijl, J. A.; Belletti, B.; and Damoni, C., 2014, "Nonlinear FEA Guideline for Modelling of Concrete Infrastructure Objects," *Computational Modelling of Concrete Structures: Proceedings of Euro-C 2014, St. Anton am Arlberg, Austria, 24-27 March 2014*, N. Bićanić, H. Mang, G. Meschke, and R. de Borst, eds., CRC Press, Boca Raton, FL, pp. 977-985.

de Boer, A.; Hendriks, M. A. N.; van der Veen, C.; and Belletti, B., 2018, "Organizing an International Blind Prediction Contest for Improving a Guideline for the Nonlinear Finite Elements Analysis of Concrete Structures," *Computational Modelling of Concrete Structures: Proceedings of the Conference on Computational Modelling of Concrete and Concrete Structures (EURO-C 2018), February 26 - March 1, 2018, Bad Hofgastein, Austria*, G. Meschke, B. Pichler, and J. Rots, eds., CRC Press, London, UK, pp. 545-552.

de Putter, A.; Hendriks, M. A. N.; Rots, J. G.; Yang, Y.; Engen, M.; and van den Bos, A. A., 2022, "Quantification of the Resistance Modeling Uncertainty of 19 Alternative 2D Nonlinear Finite Element Approaches Benchmarked against 101 Experiments on Reinforced Concrete Beams," *Structural Concrete*, early access, 15 pp. doi: 10.1002/suco.202100574

DIANA FEA BV, 2017, "DIANA User's Manual: Release 10.2," Delft, the Netherlands.

Ensink, S. W. H.; van der Veen, C.; and Hendriks, M. A. N., 2019, "Non-Linear Analysis of Prestressed Concrete T-Beams," *Advances in Engineering Materials, Structures and Systems: Innovations, Mechanics and Applications: Proceedings of the 7th International Conference on Structural Engineering, Mechanics and Computation (SEMC 2019), September 2-4, 2019, Cape Town, South Africa*, A. Zingoni, ed., CRC Press, London, UK, pp. 1360-1365.

Feenstra, P. H., 1993, "Computational Aspects of Biaxial Stress in Plain and Reinforced Concrete," PhD thesis, Delft University of Technology, Delft, the Netherlands, 159 pp.

fib, 2012, "Model Code 2010: Final Draft," Fédération internationale du béton, Lausanne, Switzerland, 676 pp.

Hordijk, D. A., 1991, "Local Approach to Fatigue of Concrete," PhD thesis, Delft University of Technology, Delft, the Netherlands, 216 pp.

Jaeger, T., and Marti, P., 2009, "Reinforced Concrete Slab Shear Prediction Competition: Entries and Discussion," *ACI Structural Journal*, V. 106, No. 3, May-June, pp. 309-318.

Lantsoght, E.; Zhang, F.; Garnica, G. Z.; Yang, Y.; and Braam, R., 2020, "Measurement Report of Prestressed Beams from Helperzoom Viaduct," Delft University of Technology, Delft, the Netherlands, 75 pp.

Lantsoght, E. O. L.; Zarate, G.; Zhang, F.; Park, M.-K.; Yang, Y.; and Sliedrecht, H., 2021, "Shear Experiments of Prestressed Concrete Bridge Girders," *ACI Structural Journal*, V. 118, No. 3, May, pp. 117-130.

Leonhardt, F.; Koch, R.; and Rostásy, F. S., 1973, "Schubversuche an Spannbetonträgern," Ernst & Sohn GmbH, Berlin, Germany.

NEN-EN 1992-1-1+C2:2011, 2011, "Eurocode 2: Design of Concrete Structures – Part 1-1: General Rules and Rules for Buildings," European Committee for Standardization, Brussels, Belgium, 246 pp.

Park, M.-K.; Lantsoght, E. O. L.; Zarate Garnica, G. I.; Yang, Y.; and Sliedrecht, H., 2021, "Analysis of Shear Capacity of Prestressed Concrete Bridge Girders," *ACI Structural Journal*, V. 118, No. 6, Nov., pp. 75-89.

Pimentel, M.; Brühwiler, E.; and Figueiras, J., 2014, "Safety Examination of Existing Concrete Structures Using the Global Resistance Safety Factor Concept," *Engineering Structures*, V. 70, July, pp. 130-143. doi: 10.1016/j.engstruct.2014.04.005

Rashid, Y. R., 1968, "Ultimate Strength Analysis of Prestressed Concrete Pressure Vessels," *Nuclear Engineering and Design*, V. 7, No. 4, Apr., pp. 334-344.

Roosen, M. A., 2017, "Ontwerp Experiment Liggers Helperzoom," Delft University of Technology, Delft, the Netherlands, 17 pp.

Rots, J. G., and Blaauwendraad, J., 1989, "Crack Models for Concrete: Discrete or Smeared? Fixed, Multi-Directional or Rotating?" *Heron*, V. 34, No. 1, pp. 1-59.

Rots, J. G.; Nauta, P.; Kuster, G. M. A.; and Blaauwendraad, J., 1985, "Smeared Crack Approach and Fracture Localization in Concrete," *Heron*, V. 30, No. 1, pp. 1-48.

RTD 1006:2013, Version 1.1, 2013, "Guidelines for the Assessment Bridges - Assessment of Structural Safety of an Existing Bridge at Reconstruction, Usage and Disapproval," Rijkswaterstaat, Utrecht, the Netherlands, 117 pp. (in Dutch)

RTD 1016-1:2020, Version 2.2, 2020a, "Guidelines for Nonlinear Finite Element Analysis of Concrete Structures," Rijkswaterstaat, Utrecht, the Netherlands, 66 pp.

RTD 1016-3A:2017, 2017a, "Validation of the Guidelines for Nonlinear Finite Element Analysis of Concrete Structures – Part 3A: Reinforced Beams," Rijkswaterstaat, Utrecht, the Netherlands, 105 pp.

RTD 1016-3B:2017, 2017b, "Validation of the Guidelines for Nonlinear Finite Element Analysis of Concrete Structures – Part 3B: Pre-stressed Beams," Rijkswaterstaat, Utrecht, the Netherlands, 113 pp.

RTD 1016-3C:2017, 2017c, "Validation of the Guidelines for Nonlinear Finite Element Analysis of Concrete Structures – Part 3C: Slabs," Rijkswaterstaat, Utrecht, the Netherlands, 129 pp.

RTD 1016-3D:2020, Version 1.0, 2020b, "Validation of the Guidelines for Nonlinear Finite Element Analysis of Concrete Structures – Part 3D: Pre-Stressed Beams 2," Rijkswaterstaat, Utrecht, the Netherlands, 109 pp.

Runzell, B.; Shield, C.; and French, C., 2007, "Shear Capacity of Prestressed Concrete Beams," Report No. MN/RC 2007-47, Minnesota

Department of Transportation Research Services Section, St. Paul, MN, 237 pp.

Schlune, H., 2011, "Safety Evaluation of Concrete Structures with Nonlinear Analysis," PhD thesis, Chalmers University of Technology, Gothenburg, Sweden, 118 pp.

Schlune, H.; Plos, M.; and Gylltoft, K., 2011, "Safety Formats for Nonlinear Analysis Tested on Concrete Beams Subjected to Shear Forces and Bending Moments," *Engineering Structures*, V. 33, No. 8, Aug., pp. 2350-2356. doi: 10.1016/j.engstruct.2011.04.008

Sun, S., and Kuchma, D. A., 2007, "Shear Behavior and Capacity of Large-Scale Prestressed High-Strength Concrete Bulb-Tee Girders," NSEL Report Series, University of Illinois at Urbana-Champaign, Urbana, IL, 147 pp.

Yang, Y.; de Boer, A.; and Hendriks, M. A. N., 2021, "A Contest on Modelling Shear Behaviour of Deep Concrete Slab Strips using Nonlinear FEM," fib *Symposium 2021: Concrete Structures: New Trends for Eco-Efficiency and Performance*, Lisbon, Portugal, 10 pp.

Zwicky, D., 2002, "Zur Tragfähigkeit stark vorgespannter Betonbalken," PhD thesis, ETH Zürich, Zürich, Switzerland, 236 pp. (in German)

Zwicky, D., and Vogel, T., 2000, "Bruchversuche an ausgebauten Brückenträgern aus Spannbeton," ETH Zürich, Zürich, Switzerland, 172 pp.

Apply for ACI Foundation Student Fellowships

ACI Foundation fellowships are offered to both undergraduate and graduate students. Students must be nominated by an ACI member faculty. Fellowships provide the following benefits:

- An educational stipend between $10,000 and $15,000 USD;
- Airfare, hotel, travel stipend, and registration for three ACI conventions;
- Assignment to an industry mentor;
- An internship, if required or desired; and
- Recognition at ACI Conventions, in *Concrete International*, and on ACI Foundation's website.

More information about ACI Foundation Fellowships is available at **acifoundation.org/scholarships**